JOURNAL OF SOLID STATE CHEMISTRY **124,** 69–76 (1996)
ARTICLE NO. 0209

The Role of Vanadium Oxide on the Titania Transformation under Thermal Treatments and Surface Vanadium States

Miguel A. Bañares,* Luís J. Alemany,* M. Carmen Jiménez,† M. Angeles Larrubia,† Fernando Delgado,† Manuel López Granados,* A. Martínez-Arias,* J. Miguel Blasco,† and José Luís G. Fierro*,[1]

Instituto de Catálisis y Petroleoquímica, CSIC, Campus UAM, Cantoblanco, E-28049-Madrid, Spain; and †Departamento de Ingeniería Química, Universidad de Málaga, E-29071-Málaga, Spain

Received August 7, 1995; in revised form February 29, 1996; accepted March 5, 1996

High surface area titania-supported materials prepared from V(*IV*) precursors and calcined at high temperatures have been characterized by Vis–UV diffuse reflectance, FT Raman, electron spin resonance, and X-ray photoelectron spectroscopies and tested in the partial oxidation of methane. Vanadium oxide loading and calcination temperature determine the structure of V_2O_5/TiO_2 materials. Below theoretical surface monolayer coverage, V(*IV*) species closely interacting with the support are observed. Vanadiam oxide species anchor by reaction with titanium oxide surface hydroxyl groups. The V(*IV*) species are stabilized by interaction with titania support and further stabilization occurs at high calcination temperatures by their location in titania (rutile) lattice. Larger loadings of vanadium decrease the temperatures required for conversion of titania (anatase) to titania (rutile). At higher vanadium loading segregation into bulk V_2O_5 oxide takes place, thus decreasing interaction with titania support. This enables a larger population of V(*V*) species than samples with surface dispersed vanadium oxide species. Although partial oxidation of methane is nonselective on titania (anatase), partial oxidation products are observed on titania (rutile)-supported vanadium oxide catalysts. The higher selectivity to partial oxidation product formaldehyde appears to be related to the high stability of V(*IV*) cations located on rutile lattice and the absence of V(*V*) sites.

INTRODUCTION

TiO_2-supported vanadium oxides have been extensively studied and used due to their high catalytic activity and selectivity in many chemical reactions (1–20). For example, V/TiO_2 is one of the most effective catalysts in the selective catalytic reduction (SCR) of NO_x by NH_3 (10, 21). In industry, usually the anatase polymorph of TiO_2 is used as a support for vanadium oxide (11). The improvement of catalytic properties obtained by the use of anatase as a support has been explained by the formation of highly dispersed vanadia species. As the interaction between vanadium oxide and titania support takes place essentially by anchoring V(*IV*) species on titania support, the use of V(*IV*) precursors is expected to result in better dispersion of vanadium oxide species. Simultaneously, a better interaction of vanadium oxide species with titania support appears to promote anatase to rutile transformation at lower temperatures than for a vanadium oxide free titania (anatase) (15). The metal oxide–support interaction is weaker on titania (rutile) than on titania (anatase) as evidenced by the smaller monolayer dispersion capacity of titania (rutile) *vs* titania (anatase). The lower dispersion capacity appears to be essentially related to the lower amount of surface hydroxyl groups present on titania (rutile) phase.

Partial oxidation of methane on supported metal oxides is quite a challenging field (22–26). Few oxides have proved to be active for converting methane into C_1-oxygenates, however only silica support appears to be appropriate for the selective conversion of methane. The use of other supports promote, in general, nonselective oxidation reactions of methane (27, 28). The effect of the support on the catalytic performance in the case of methanol oxidation reactions appears to be related to the reducibility of the supported metal oxide (29). For the selective oxidation of methane, however, the situation is more complex as the redox properties of the system do not relate to their catalytic functionality (30, 31). Results presented provide a possible explanation for the different reactivity in methane oxidation for the presence of vanadium oxide catalysis.

EXPERIMENTAL DETAILS

Titania support samples have been prepared by neutralization to pH 6 of an acid solution of high purity grade $TiCl_4$. The precipitate after filtering and washing with water to remove chloride ions has been dried overnight at 383 K and calcined at 873 K. Titania-supported vanadia

[1] To whom correspondence should be addressed.

0022-4596/96 $18.00

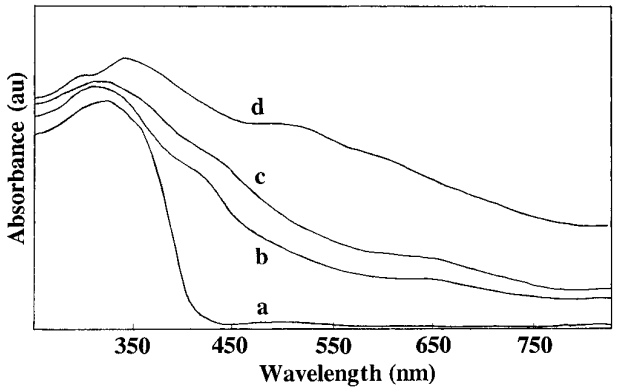

FIG. 1. UV–Vis DRS spectra of (a) TiO_2, (b) 1.5VTi-873 K, (c) 3.5VTi-873 K, and (d) 7.5VTi-873 K. $BaSO_4$ was used as a reference.

samples have been prepared by dry impregnation technique with a hot water solution of ammonium metavanadate and oxalic acid (Merk, reagent grade) as complexing agent with V_2O_5 nominal loadings of 0.3, 1.5, 3.5, and 7.5%. Afterward, the samples were dried and calcined at 873, 973, and 1073 K. The samples will be referred hereafter as xVTi-TK, where x is the nominal V_2O_5 loading and T is the calcination temperature in Kelvin. For instance, the 3.5 VTi-973 K sample is a vanadia–titania catalyst containing 3.5% V_2O_5 and calcined at 973 K.

UV–Vis diffuse reflectance of the materials under ambient conditions were performed on a Kontron UVIKON 810 spectrophotometer equipped with an integrating sphere using $BaSO_4$ as a reference. ESR spectra were recorded at 77 K with a Bruker ER 200D spectrometer operating in the X-band. A modulation of 100 kHz and a

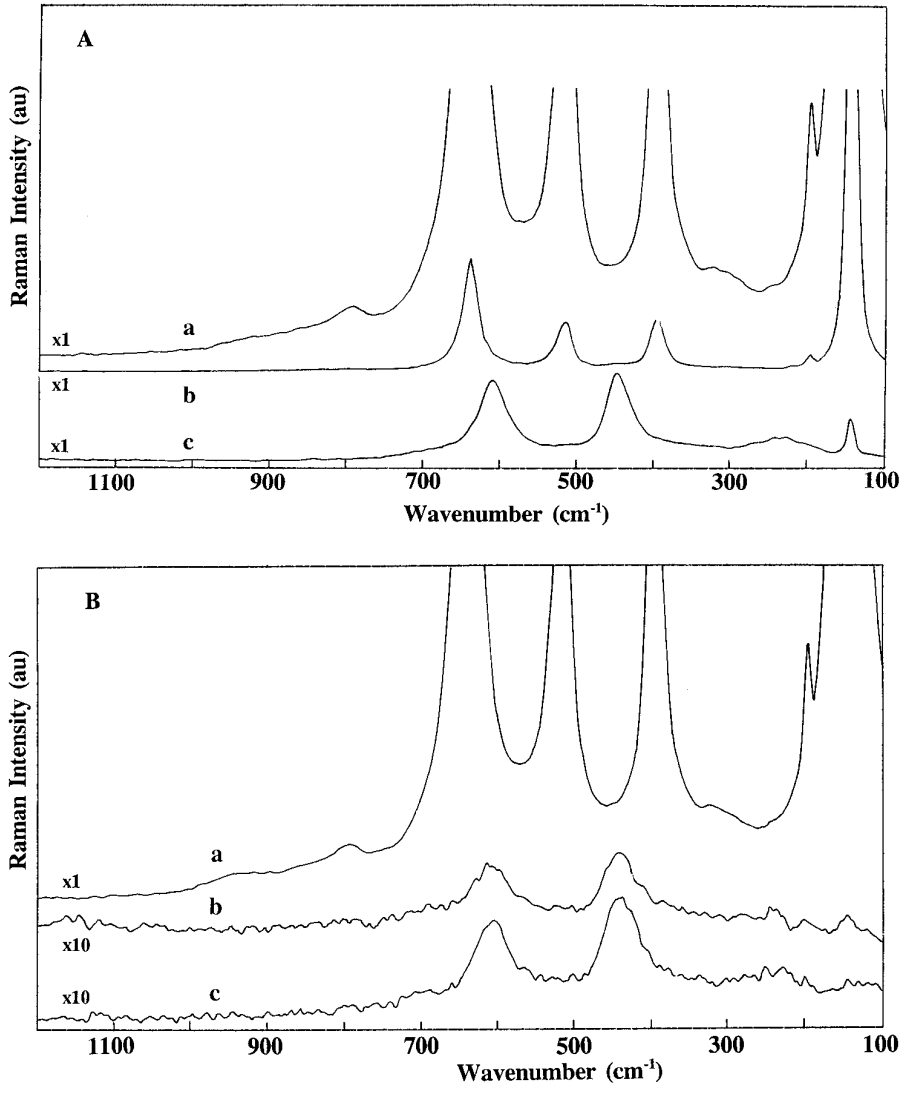

FIG. 2. Ambient FT-Raman spectra of catalysts 0.3VTi (a), 3.5VTi (b), and 7.5VTi (c) treated at 873, 973, and 1073 K. Magnification factors are indicated in figures.

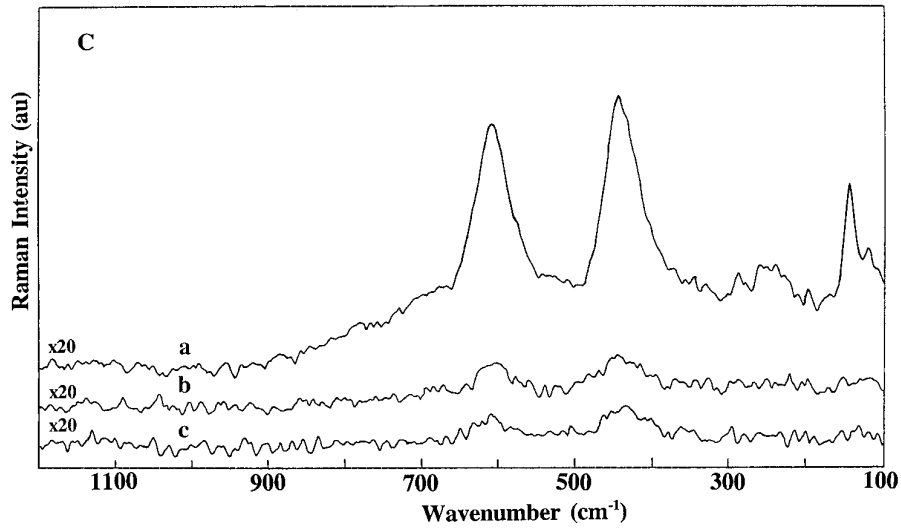

FIG. 2—*Continued*

DPPH standard with $g = 2.0036$ were used. Powder samples of ca. 40 mg were placed in a vacuum quartz cell assembled with greaseless stopcocks capable of maintaining a dynamic vacuum below 10^{-4} Torr (1 Torr = 133.33 N/m^2). The sample was outgassed at room temperature. Pulses of oxygen were dosed at 77 K on samples previously evacuated. Spectra were recorded at 77 K. Quantification of V(*IV*) centers detected was done by double integration of the ESR signal. The results were compared with those of a known amount of $CuSO_4 \cdot 5H_2O$ (a standard for spins quantification). Raman spectra were obtained with a Bruker FT-Raman instrument using the 1064 nm exciting line. Samples were placed in stationary sample holders and kept in the ambient environment. The power was fixed to the range 20–40 mW in order to avoid sample vaporization. Photoelectron spectra were obtained with a Fisons ESCALAB 200 R spectrometer equipped with a Mg$K\alpha$ X-ray source ($h\nu$ = 1253.6 eV) and a hemispherical electron analyzer. The powder samples were pressed into stainless steel cylinders and mounted on a long rod which allows transfer from the preparation chamber. Energy region of the photoelectrons were scanned at a pass energy of 20 eV. For each sample, C 1*s*, O 1*s*, Ti 2*p* , and V 2*p* peaks were recorded. Although surface charging was observed in all samples, accurate binding energies (±0.2 eV) could be determined by charge reference to the C 1*s* peak at 284.5 eV.

Partial oxidation of methane was performed at atmospheric pressure. The reactor consisted of a 6 mm o.d. quartz tubing and minimum dead volume in the reactor after the bed of the catalyst to prevent furter degradation of partial oxidation products (32). Methane and oxygen were cofed in a molar ratio of 2.0 and the reactor effluents were analyzed by an on-line GC Hewlett–Packard Mod. HP-5890-II with a Chromosorb 107 and molecular sieve 5A packed columns and a TC detector.

RESULTS

The Vis–UV DR spectra of V_2O_5/TiO_2 samples calcined at 873 K are shown in Fig. 1. TiO_2 support absorbs in the ultraviolet region, 320–350 nm, due to an electron transition from valence band to a higher band, Incorporation of vanadia yields absorption in the 400–440 nm region and a broad feature which extends over the whole visible region with a maximum at ca. 650 nm. The new profiles increase as vanadium oxide loading increases. After subtraction of the TiO_2 contribution a single maximum near 400 nm characteristic of surface vanadium oxide species is present for the lowest vanadium coverages. As the vanadium content increases a new absorption band is observed at 430 nm. Bands at lower energies must originate from octahedrally coordinated surface vanadium oxide species which absorb at lower energy than tetrahedrally coordinated ones. The 7.5VTi-873 K sample presents bands at ca. 320 and 350 cm^{-1} associated to rutile phase (15) and a band centered at 450, as well as a broad feature above ca. 550 nm associated to bulk V_2O_5 (33, 34).

The effect of vanadium oxide loading and calcination temperature of the VTi materials was studied by FT-Raman spectroscopy under ambient conditions (Fig. 2). The Raman bands observed at 643, 515, 401, 197, and 152 cm^{-1} for 0.3 VTi calcined at 873 K (Fig. 2a) are characteristic of titania (anatase) phase (35). No significant differences could be observed for 0.3VTi when calcination temperature is increased to 973 K but calcination of this sample

TABLE 1
XPS Characterization of V_2O_5/TiO_2

Sample	O 1*s*	Ti $2p_{3/2}$	V $2p_{3/2}$	I_V/I_{Ti}
0.3VTi-873 K	529.9	458.5	517.4 (47)	0.074
	531.1		516.3 (53)	
	533.3			
3.5VTi-873 K	529.7	458.5	517.2 (58)	0.175
	531.4		516.2 (42)	
	532.8			
7.5VTi-873 K	530.0	458.7	517.3 (63)	0.403
	531.6		516.3 (37)	
0.3VTi-973 K	529.9	458.5	516.2	0.130
3.5VTi-973 K	530.1	458.5	517.1 (58)	0.218
			516.2 (42)	
7.5VTi-973 K	529.9	458.5	517.1 (69)	0.415
			516.2 (31)	
0.3VTi-1073 K	529.9	458.5	516.0	0.060
3.5VTi-1073 K	530.0	458.5	516.3	0.071
7.5VTi-1073 K	529.9	458.5	516.1	0.086

Note. Values in parentheses indicate the percentage of a given peak.

at 1073 K presents different Raman bands at ca. 609, 447, 226, and 142 cm^{-1}, characteristic of the rutile (titania) (35). The 3.5VTi catalyst displays behaviour similar to that of its 0.3VTi homing but transition to rutile phase is observed after calcination at 973 K (Fig. 2b). The presence of rutile phase is already observed after calcination at 873 K for 7.5VTi (Fig. 2c). In addition, some very weak features at ca. 992, 956, 550–400, 289, 262, 196, and 120 cm^{-1} may be indicative of very small crystallites of V_2O_5 (36, 37). The promotional effect of vanadium oxide in anatase to rutile transformation has been reported (38–40) and appears to proceed via surface reaction with titanium sites which could be governed by a mechanism of grain growth (41).

The XPS characterization results for samples calcined at 873 K are presented in Table 1. The binding energy of the most intense Ti $2p_{3/2}$ core level at 458.7 eV is characteristic of TiO_2 support (13, 42). The 01*s* core level spectra shows a major component at 529.7–530.0 eV associated to lattice oxygen (O^{2-}) of titania substrate and a minor one at ca. 531.5 eV, characteristic of surface hydroxyl groups on titania surface, which is similar to that found on transition metals hydroxides and oxides (42). Moreover, a third weak component at higher BE (ca. 533 eV) is observed in a few instances due to adsorbed molecular water. The presence of molecular water is only observed in two samples (Table 1) and the intensity of its signal is less than 7% of the total O 1*s* signal, and always lower than that of O 1*s* from surface hydroxyl groups. No differences associated to this amount of water are observed with respect to the other samples where no molecular water is present. The intensity of the band at 531.5 eV decreases with increasing vanadium loading (Fig. 3). This strongly suggests that vanadium species anchor on titania support by reaction with surface hydroxyl groups in a similar fashion to other supported metal oxide systems (43–46). In fact, a comparison between theoretical surface coverage and remaining surface hydroxyl groups has remarkably good correlation ($R = 0.999$), which evidences the role of surface hydroxyl groups in dispersing supported oxides. By applying peak synthesis procedures, the V $2p_{3/2}$ core level spectra display two components at 517.3 eV, very close to V(*V*) species, and at 516.3 eV, characteristic of V(*IV*) species (13). The V(*IV*)/V(*V*) XPS population ratios of the materials calcined at 873 K (Table 1) show that below monolayer surface coverage vanadium oxide species are essentially like V(*IV*). Under XPS analysis conditions photoreduction of vanadium is also expected. However, the amount of V(*IV*) recorded on samples prepared with V(*V*) precursors typically show 15–20% of V(*IV*). V(*IV*) recorded by XPS here is 30–50%. This must be indicative of the presence of reduced vanadium species prior to XPS measurements.

The XPS V/Ti atomic ratio increases linearly with vanadium oxide loading (Table 1). This is indicative of an essentially well dispersed vanadium oxide phase where vanadia aggregates are not bigger than 4 nm. The small size of vanadia crystals can be inferred from the very weak V_2O_5 Raman features observed. The V(*IV*)/V(*V*) ratio of 7.5VTi (0.59) is indicative that a large amount of vanadium sites still interact closely with titania support. There is a band broadening with increasing vanadium oxide loading which is also indicative of a higher heterogeneity in the nature of the titania-supported vanadium oxide species.

Vanadium oxide loading on titania determines different

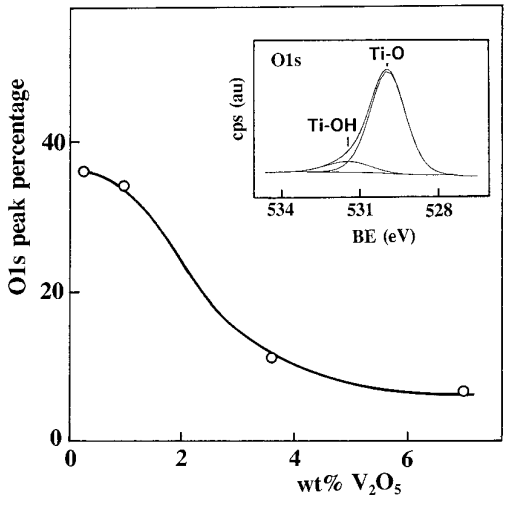

FIG. 3. Evolution of XPS O 1*s* peak percentage as a function of vanadium loading for samples calcined at 873 K. Inset figure presents the binding energy region deconvolution for O 1*s* for surface hydroxyl groups and lattice titania.

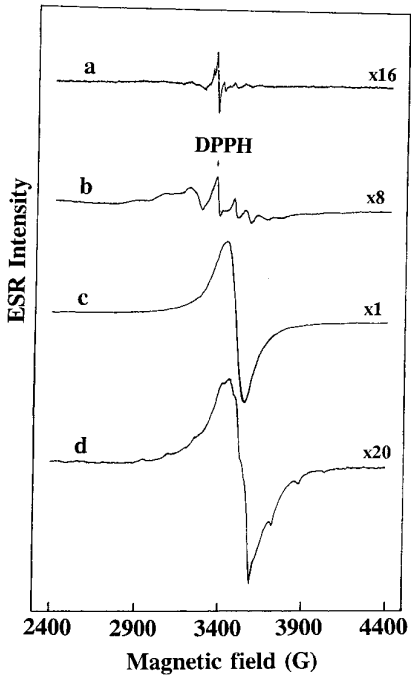

FIG. 4. ESR spectra of representative (a) 0.3VTi-873 K, (b) 3.5VTi-873 K, (c) 4.5VTi-873 K, and (d) 3.5VTi-1073 K materials. Magnification factors are indicated in the figure.

ESR spectra (Fig. 4a–4d) for a given temperature. Sharp hyperfine signals are observed at low surface vanadium oxide loading indicating isolated V(*IV*) sites. The axial signal is associated with vanadyl VO^{2+} or V^{4+} isolated centers (7–10). The amount of V(*IV*) centers on this sample is ca. 10% of all supported vanadium oxide for 0.3VTi-873 K (Fig. 4a). All V(*IV*) present is likely to be detected by ESR since presumably no V–V interactions are present at this lower vanadium loading. This accounts for the larger degree of reduction observed by XPS. At higher loading, the V–V interaction increases as evidenced by dipolar broadening interaction (10–12). At higher vanadium coverages vanadyl octahedral species are dominant. 7.5VTi presents an ESR spectral envelope characteristic of V(*IV*) in octahedral environment which may arise from V(*IV*) cations in the octahedral lattice of titania (rutile) or in the V_2O_5 lattice since the presence of vanadium cations with a lower oxidation state is common in V_2O_5 (47). In addition, the absence of Ti(*III*) in ESR spectra strongly supports the proposed close interaction between both oxides. This interaction prevents reduction of titania support thus yielding ESR spectra where only vanadium sites are recorded.

Figure 5 presents the evolution of the ESR signal of 3.5VTi-873 K evacuated at room temperature (Fig. 5a) and treated with a pulse of oxygen at 77 K (Fig. 5b). The intensity of the ESR signal significantly decreases. Additional pulses of oxygen do not decrease the ESR signal

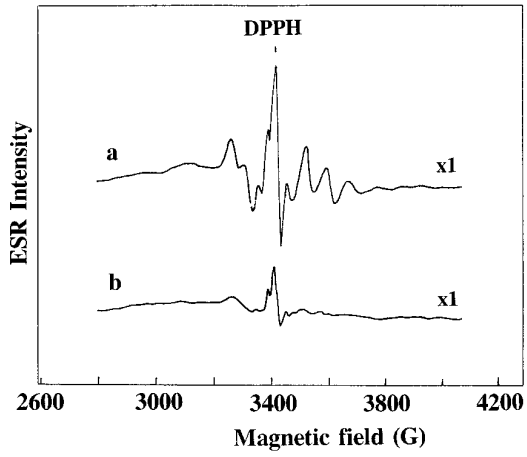

FIG. 5. ESR spectra of 3.5VTi-873 K (a) evacuated at room temperature and at 10^{-4} Torr; (b) Sample (a) after a pulse of oxygen at 77 K.

any more. The dipolar interaction of paramagnetic oxygen with surface paramagnetic centers visible by ESR broadens and even depletes the ESR signal by dipolar interaction (50). Since bulk paramagnetic centers are not affected by oxygen adsorption, the remarkable decrease presented above for the ESR signal clearly evidences that most of V(*IV*) centers are located in the surface. Since additional oxygen pulses did not further decrease the ESR signal of the V(*IV*) species, the remaining V(*IV*) species detected by ESR are not located at the surface. They are probably located in the subsurface layers.

Methane conversion on VTi materials yields essentially CO and CO_2 products. No partial oxidation products can be observed on 3.5VTi-873 K. However 7.5VTi-873 K does show some production of formaldehyde (Table 2). In addition 3.5VTi-1073 K is much less reactive than 3.5VTi-873 K. However, formaldehyde is the most selective oxidation product. At conversion levels close to those reported for 3.5VTi-873 K (Table 2) formaldehyde is still produced (Fig. 6). Formaldehyde production for 3.5VTi-1073 K is higher than for 7.5VTi-873 K as the temperature increases (Fig. 6). In general nonselective oxidation products are

TABLE 2
Methane Conversion Activity

	% Conversion		% Selectivity		
Catalyst	CH_4	O_2	CO	CO_2	HCHO
3.5VTi-873 K	1.66	2.19	87.2	12.8	0.0
7.5VTi-873 K	0.08	0.68	80.0	14.1	5.9
3.5VTi-1073 K	0.01	0.25	0	0	100

Note. Reaction conditions: 803 K; $W/F = 1.2$ gh/mol; $CH_4/O_2 = 2$ molar.

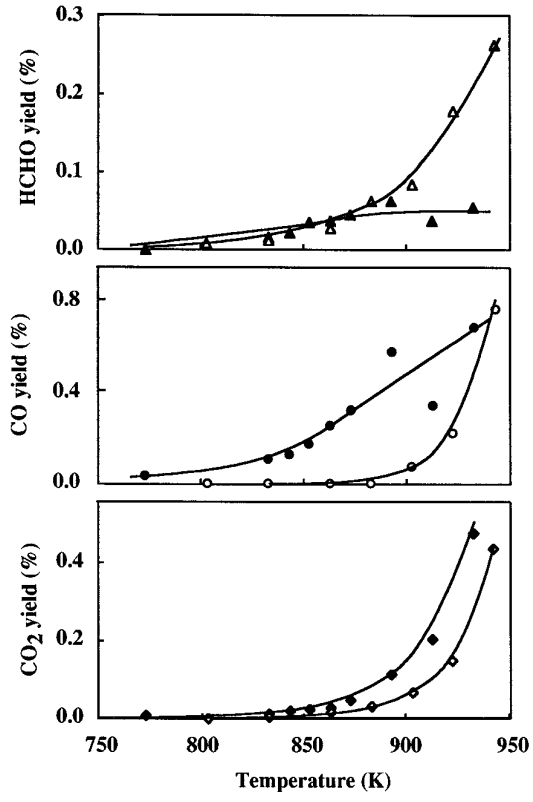

FIG. 6. Yield to CO (O), CO2 (◇), and HCHO (△) on catalyst 7.5VTi-873 K and 3.5VTi-1073 K vs reaction temperature. Reaction feed CH_4/O_2 = 2 molar, methane pseudo-residence time = 1.2 g · h/mol.

more favored on 7.5VTi-873 K. As methane conversion increases, production of CO_x products becomes dominant.

DISCUSSION

The structures of vanadium oxide and titania on V_2O_5/TiO_2 materials are strongly affected by vanadium oxide loading and temperature treatment. Vanadium oxide interacts strongly with the titania support. For a given temperature (873 K), vanadium oxide is present as isolated tetrahedral V(*IV*) species. The progressive consumption of titania surface hydroxyl groups as vanadium oxide increases (Fig. 3) evidences the role of –OH groups in anchoring vanadium oxide. Vanadium oxide, as V(*V*) species, is essentially dispersed, as suggested by the V/Ti XPS ratio trend and confirmed by ESR spectroscopy. This strong interaction between both oxides originates from the stabilization of V(*IV*) cations in the titania surface due to the remarkably close radii ratio (V(*IV*)/Ti(*IV*) = 0.063 nm/0.068 nm). Therefore, it appears that V(*IV*) species are essentially associated to surface dispersed vanadium oxide sites closely interacting with titania support for 0.3VTi-873 K. This behavior differs from V/TiO_2 materials prepared from V(*V*) precursors (18). As vanadium oxide loading increases the amount of available surface hydroxyl groups decreases and anchorage of vanadium oxide on titania support becomes less favorable. The increase in V(*V*) species corresponds to the almost complete removal of surface hydroxyl groups. At the highest vanadium oxide loading formation of bulk V_2O_5 is evident. Transition from isolated dispersed V(*IV*) species to bulk V_2O_5 takes place in a progressive manner. ESR evidences increasing V–V interaction that results from segregation of dispersed isolated vanadium oxide species yielding crystals of V_2O_5 at the highest loading (ESR, DRS, and FT-Raman). The size of V_2O_5 crystals is not very large as inferred from the very weak Raman features and the essentially linear increase of the V/Ti XPS intensity ratio, even at the highest vanadium oxide loading. Consequently, V_2O_5 crystals are not expected to be larger than 4 nm. The progressive decrease for the V(*IV*)/V(*V*) ratio originates from the weaker interaction of aggregated vanadium oxide and bulk V_2O_5 crystals with titania support.

The transformation of titania (anatase) into titania (rutile) phase is favored by increasing vanadium oxide loading or calcination temperature. Pure titania (anatase) transforms into rutile at ca. 1200 K (40). However, transition to rutile takes place at remarkably lower temperatures on V_2O_5/TiO_2 materials. In addition, as vanadium oxide loading increases, the temperature required to render transition to rutile decreases. ESR measurements for 7.5VTi-1073 K show the existence of V(*IV*) in octahedral coordination. V(*IV*) cations could be located in V_2O_5 lattice or integrated into the octahedral lattice of rutile. Both options appear to be possible for the sample with rutile phase calcined at 873 K (7.5VTi-873 K). ESR, FT-Raman, and DRS show the existence of small crystals of V_2O_5. V(*IV*) cations are present in the octahedral lattice of V_2O_5 which possesses nonstoichiometric structures (47). However, V(*IV*) cations may also locate in the interstitial sites of titania crystal lattice. Heat treatments may promote diffusion of V(*IV*) into titania crystal structure thus generating substitutional defects. They must act like initiation nuclei for $V_xTi_{1-x}O_2$ (rutile) phase genesis, which is almost identical to pure titania (rutile) phase (38, 39). Since V(*IV*) and titania (rutile) phase are highly soluble (48), this promotional effect should not have a limit. Monolayer surface coverage of vanadium on the titania support should be the only limitation. However, once vanadium diffusion into titania initiates, segregated vanadium oxide species could also diffuse into rutile lattice. As vanadium oxide loading on titania increases, transition to rutile happens at lower temperatures. Since vanadium oxide species are essentially dispersed and closely interacting with titania support, a higher vanadium oxide loading results in a higher surface density of initiation nuclei for transformation into rutile (41). V_2O_5/TiO_2 samples with low vanadium oxide loading

will require high calcination temperatures to promote transformation into rutile phase. ESR spectra do show the modification for the environment of vanadium cations after calcination of 3.5VTi-873 K at 1073 K (Fig. 4). No segregated vanadium oxide species appear to be present for this sample since no V(*V*) is recorded by XPS and no Raman features or ESR signal evidence V–V interaction. In addition, V/Ti XPS intensity ratios after 1073 K treatment decrease due to diffusion of vanadium from the surface to titania lattice. The ESR signal recorded for 3.5VTi-1073 K corresponds to V(*IV*) cations located only exclusively in octahedral rutile lattice. It is almost identical to the ESR spectrum of 7.5VTi-873 K, where V(*IV*) cations may be located on rutile or vanadia lattices. The modifications induced on rutile lattice by diffusion of vanadium oxide into rutile phase (38, 49) can clearly be observed by Raman spectroscopy. They show that as vanadium oxide loading increases the resulting Raman bands for rutile phase broaden and are weaker due to the worse definition of rutile vibrational modes.

Different environments generated for vanadium cations have outstanding effects on the reactivity of V_2O_5/TiO_2 materials for methane oxidation. Highly dispersed vanadium oxide on titania anatase does not yield any selective oxidation product (formaldehyde). However, transformation into rutile phase appears to give partial oxidation products. The 3.5VTi–1073 K is much less reactive than the other materials. On the other hand, selective oxidation is much higher. From the comparison of the two catalysts that yield selective oxidation products (Fig. 6) it is evident that 3.5VTi-1073 K is more selective than 7.5VTi-873 K in all the reaction temperature range. The main difference between these two materials is that no V(*V*) is present on the most selective one. In fact, V(*IV*) is so much stabilized by titania that no V(*V*) can be observed even after calcination in air at 1073 K. The high stability of V(*IV*) in the titania (rutile) lattice has already been observed (4). This may be the origin for the higher selectivity of 3.5VTi-1073 K: methane activation takes place by reaction with oxygen either in the gas phase (homogenous reaction) or promoted by the surface area of the support. Supported vanadium oxide (predominantly V(*V*)) undergoes some reduction during the methane oxidation reaction, as *in situ* Raman spectroscopy evidences (27). A slight degree of reduction, as is the case for V_2O_5/SiO_2 catalysts, provides sites for oxygen adsorption and therefore activation. However, vanadium oxide supported on reducible oxide (TiO_2, SnO, etc.) undergoes larger reduction that excessively increases the amount of activated oxygen thus yielding nonselective oxidation products (27). For 3.5VTi-1073 K all vanadium is present like V(*IV*) in a rutile lattice which does not have any tendency to be oxidized. Thus, no oxygen activation is expected and this may account for the higher selectivity toward partial oxidation products.

CONCLUSIONS

Vanadium loading and temperature treatments determine the nature of supported vanadia species and titania support. Vanadium oxide species interact closely with titania support and are stabilized as V(*IV*). V(*IV*) cations are incorporated into the TiO_2 crystal lattice by substitutional defects which induces formation of rutile phase. Consequently, surface V(*IV*) sites act as initiation nuclei for rutilation of the titania (anatase) phase. As vanadium oxide loading increases the temperature required to transform titania support into rutile phase decreases. Since V(*IV*) can dissolve in titania (rutile), as isomorphic substitution by V(*IV*) into the rutile lattice increases, rutile structure is modified and loses its crystallinity. Formation of V(*V*) species at high vanadia loading appears to be associated to segregated vanadium oxide species where interaction with titania support is weaker. However, as calcination temperature is increased, diffusion of vanadia cation into rutile anatase is promoted. $V_xTi_{1-x}O_2$ (rutile) materials where all vanadium is in titania lattice makes them more selective for methane conversion since no oxygen activation sites are provided, as compared to $V_xTi_{1-x}O_2$ materials where surface segregated vanadium oxide species are still present.

ACKNOWLEDGMENTS

The authors appreciate the help of Mr. F. Sánchez Constela in performing ESR spectra. M. A. B. thanks European Union for Grant JOU2-CT93-0354. Financial support by CICYT (Projects AMB93-1426 and MAT95-0894) are gratefully acknowledged.

REFERENCES

1. G. Busca, G. Centi, L. Marchetti, and F. Trifiró, *Langmuir* **2,** 568 (1986).
2. J. L. G. Fierro, L. A. Gambaro, A. R. González-Elipe, and J. Soria, *J. Colloid Surf.* **11,** 31 (1984).
3. G. Busca, L. Marchetti, G. Centi, and F. Trifiró, *J. Chem. Soc. Faraday Trans.* **81,** 1003 (1985).
4. K. Dryek, E. Serwicka, and B. Gryzwoska, *React. Kinet. Catal. Lett.* **10,** 93 (1979).
5. M. Rusiecka, B. Grzybowska, and M. Gasior, *Appl. Catal.* **10,** 101 (1984).
6. K. V. R. Chary, Malupal, B. Reddy N. K. Nag, V. S. Subrahmanyam, and C. S. Sunandana, *J. Phys. Chem.* **88,** 2622 (1984).
7. G. C. Bond and A. J. Sarkany, *J. Catal.* **57,** 476 (1979).
8. M. C. Jiménez, L. J. Alemany, M. A. Bañares, F. Delgado, J. M. Blasco, submitted for publication.
9. G. C. Bond and S. Flamerz, *Appl. Catal.* **71,** 1 (1991).
10. H. Bosch and F. Janssen, *Catal. Today* **2,** 369 (1988).
11. S. Matsuda and A. Kato, *Appl. Catal.* **8,** 149 (1983).
12. M. Gasior, J. Haber, and T. Machej, *Appl. Catal.* **33,** 1 (1987).
13. G. A. Sawatzky and D. Post, *Phys. Rev. B* **20,** 1546 (1979).
14. S. Jansen, Y. Tu, M. J. Palmieri, M. Sanati, and A. Andersson, *J. Catal.* **138,** 79 (1992).
15. L. J. Alemany, F. Delgado, and J. M. Blasco, *React. Kinet. Catal. Lett.* **53,** 1 (1994).

16. F. Roozeboom, A. J. Van Dillen, J. W. Geus, and P. J. Gellings, *Ind. Eng. Chem. Prod. Res. Dev.* **21,** 304 (1981).
17. H. Knözinger and E. Taglauer, *Catalysis* **10,** 1 (1993).
18. J. Haber, T. Machej, E. M. Serwicka, and I. E. Wachs, *Catal. Lett.* **32,** 101 (1995).
19. J. M. Gallardo Amores, V. Sánchez Escribano, G. Busca, and V. Lorenzelli, *J. Mater. Chem.* **4(6),** 965 (1994).
20. J.-M. Jehng and I. E. Wachs, *Catal. Lett.* **13,** 9 (1992).
21. Y. Cai and U. S. Ozkan, *Appl. Catal.* **78,** 241 (1991).
22. H.-F. Liu, R.-S. Liu, K. Y. Liew, R. E. Johnson, and J. H. Lunsford, *J. Am. Chem. Soc.* **106,** 4117 (1984).
23. N. D. Spencer and C. J. Pereira, *J. Catal.* **116,** 399 (1989).
24. Q. Sun, J. I. di Cosimo, R. G. Herman, K. Klier, and M. Bashin, *Catal. Lett.* **15,** 371 (1992).
25. A. Parmaliana, V. Sokolovski, D. Miceli, F. A. Arena, and N. Giordano, *J. Catal.* **148,** 514 (1994).
26. M. A. Bañares, J. L. G. Fierro, and J. B. Moffat, *J. Catal.* **142,** 406 (1993).
27. Q. Sun, J.-M. Jehng, H. Hu, R. G. Herman, I. E. Wachs, and K. Klier, ''Symposium on Methane and Alkane Conversion Chemistry.'' San Diego ACS Conference, March 1994.
28. M. A. Bañares, B. Pawelec, and J. L. G. Fierro, *Zeolites* **12,** 882 (1992).
29. I. E. Wachs, G. Deo, D. S. Kim, M. A. Vuurman, and H. Hu, *in* ''New Frontiers in Catalysis'' (L. Guczi *et al.*, Eds.). Elsevier, Amsterdam, 1992.
30. M. A. Bañares, N. D. Spencer, M. D. Jones, and I. E. Wachs, *J. Catal.* **146,** 204 (1994).
31. M. Faraldos, M. A. Bañares, J. A. Anderson, H. Hu, I. E. Wachs, and J. L. G. Fierro, *J. Catal.* in press.
32. M. A. Bañares and J. L. G. Fierro, *in* ''Catalytic Selective Oxidation'' (S. T. Oyama and J. H. Hightower, Eds.), Chap. 23, ACS Symposium Series 523. *Am. Chem. Soc.,* Washington, DC, 1993.
33. H. Praliaud and M. J. Mathieu, *J. Chim. Phis.* **73,** 689 (1973).
34. G. Busca and A. Zecchina (Compilers), *Catal. Today* **20,** 61 (1994).
35. G. Deo, A. M. Turek, I. E. Wachs, T. Machej, J. Haber, N. Das, H. Eckert, and A. M. Hirt, *Appl. Catal.* **91,** 27 (1992).
36. C. C. Williams, J. G. Eckerdt, J. M. Jehng, F. D. Hardcastle, A. M. Turek, and I. E. Wachs, *J. Phys. Chem.* **95,** 878 (1993).
37. J. Engweiler and A. Baiker, *Appl. Catal.* **120,** 187 (1994).
38. R. Y. Saleh, I. E. Wachs, S. S. Chan, and C. C. Chersich, *J. Catal.* **98,** 102 (1986).
39. G. Hausinger, H. Schmelz, and H. Knözinger, *Appl. Catal.* **39,** 267 (1988).
40. B. E. Handy, M. Maciejewski, and A. Baiker, *J. Catal.* **134,** 75 (1992).
41. L. Rey, R. Martino, L. Gambaro, and H. Thomas, *Rev. Latin. Ing. Quím. Apl.* **16,** 231 (1986).
42. D. Briggs and M. P. Seah (Eds.), ''Practical Surface Analysis. Auger and X-Ray Photoelectron Spectroscopy.'' Wiley, Chichester/New York, 1991.
43. L. J. Alemany, R. Mariscal, M. Galán-Fereres, M. A. Bañares, J. A. Anderson, and J. L. G. Fierro, *Chem. Mater.* **7,** 1342 (1995).
44. Z. Liu, J. Tabora, and R. J. Davis, *J. Catal.* **149,** 117 (1994).
45. T. -Ch. Liu, M. Forissier, M. Coudurier, and J. C. Vèdrine, *J. Chem. Soc. Faraday Trans. I* **85,** 1607 (1989).
46. R. D. Roark, S. D. Kohler, and J. G. Ekerdt, *Catal. Lett.* **16,** 71 (1992).
47. N. N. Greenwood and A. Earnshaw, ''Chemistry of the Elements,'' Chap. 22. Pergamon Press, Oxford, 1989.
48. F. Maillot and R. A. Davis, *C. R. Acad. Sci. Paris Ser. C* **277,** 1361 (1973).
49. P. Lostak, Z. Cernosek, E. Cernoskova, L. Benes, J. Kroutil, and V. Rambousek, *J. Mater. Sci.* **28,** 1189 (1993).
50. M. Che and Giamello, in ''Spectroscopic Characterization of Heterogeneous Catalysts,'' (J. L. G. Fierro, Ed.) p. B293. Elsevier, Amsterdam, 1990.